Nano Research 2014, 7(10): 1488–1496
DOI 10.1007/s12274-014-0510-3
Research Article
ISSN 1998-0124
CN 11-5974/O4

Dual functional transparent film for proximity and pressure sensing

Bo Zhang[1,§], Zemin Xiang[1,§], Siwei Zhu[1], Qiyi Hu[1], Yuanzhi Cao[1], Junwen Zhong[1], Qize Zhong[1], Bo Wang[1,2], Yunsheng Fang[1], Bin Hu[1] (✉), Jun Zhou[1], and Zhonglin Wang[3]

[1] *Wuhan National Laboratory for Optoelectronics (WNLO), School of Optical and Electronic Information, Huazhong University of Science and Technology (HUST), Wuhan 430074, China*
[2] *Department of Electrical Engineering and Automation, Luoyang Institute of Science and Technology, Luoyang 471023, China*
[3] *School of Materials Science and Engineering, Georgia Institute of Technology, Atlanta, Georgia 30332-0245, USA*
§ *These authors contributed equally to this work.*

Received: 14 April 2014
Revised: 3 June 2014
Accepted: 7 June 2014

KEYWORDS
proximity sensor,
pressure sensor,
mutual capacitance,
silver nanowire,
transparent film

ABSTRACT

Over the past few years, the rapid development of tactile sensing technology has contributed significantly to the realization of intuitional touch control and intelligent human–machine interaction. Apart from physical touch or pressure sensing, proximity sensing as a complementary function can extend the detection mode of common single functional tactile sensors. In this work, we present a transparent, matrix-structure dual functional capacitive sensor which integrates the capability of proximity and pressure sensing in one device, and the excellent spatial resolution offered by the isolated response of capacitive pixels enables us to realize precise location identification of approaching objects and loaded pressure with fast response, high stability and high reversibility.

1 Introduction

Planar touch sensors, as the pivotal component of accessible man–machine interaction systems, are capable of recognizing tactile information through monitoring either capacitance or resistive change, and they have promoted the revolutionary development of portable electronics [1]. Recent advances, from device design to manufacturing techniques, have endowed the touch sensor with various novel characteristics, including high flexibility [2, 3], high pressure sensitivity [4], high spatial-resolution [5], and even self-healing capability [6] to mimic the properties of natural skin by electronic or optical means [7, 8]. For these devices, physical

Address correspondence to Bin Hu, bin.hu@hust.edu.cn

contact between sensors and objects is essential for triggering the response regardless the applied weight and shape of the objects, e.g., as contact-mode-based sensors that are "blind" to the approaching objects. To address this issue, proximity sensing as a complementary function can be incorporated into such artificial skin to provide a dual functional sensing capability [9–11], which could expand the applications of common single functional pressure sensors—for instance helping robots to detect objects for collision avoidance and take pre-action in the dark, or enabling a smart phone to sense the hovering fingers with accurate positions and distance from the screen. Among different detection mechanisms, such as infrared light, ultrasonic waves and magnetic induction [12, 13], proximity sensors based on capacitance measurement are attractive considering their easy fabrication and integration [14], and can detect an approaching object whilst being insensitive to the colour and texture. On the other hand, capacitance change monitoring can also be used for pressure sensing and has been widely studied [15–18]. Therefore, finding an economical and efficient way to merge isolated capacitance-based pressure sensors and proximity sensors in one device with seamless response and switching can add more functions to the sensors.

Here in this work, based on the widely used orthogonally patterned electrodes structure, we studied the continuous response of pressure and proximity sensing using a highly transparent film. The device is capable of quantitatively detecting and distinguishing objects in three different states—namely proximity, contact and pressure-loading—by monitoring the capacitance change between two transparent electrodes made of a silver nanowire (AgNWs) network [19–21]. Moreover, we demonstrated that the device has good multiple point spatial resolution in proximity mode, something which has rarely previously been reported.

2 Result and discussion

As shown in the schematic illustration in Fig. 1(a), the capacitive sensor was designed as a sandwich structure, as employed in many previous studies [22–25]. A polyethylene terephthalate (PET) sheet was used as the substrate with parallel electrode stripes patterned on it. Two such PET substrates were bonded together using elastic polydimethylsiloxane (PDMS) as the dielectric layer with top and bottom electrode stripes placed orthogonally (row-and-column electrodes). In the pursuit of high transparency to satisfy the requirements of touch screen applications [26], an AgNWs network was selected as the electrode [27, 28], and was assembled by crossing AgNWs (Fig. 1(b)) with diameters and lengths around 200 nm and hundreds of micrometers (Figs. S1(a) and S1(b), in the Electronic Supplementary Material (ESM)). The mechanical robustness and conductivity could be improved by self-welding of AgNWs junctions after plasma irradiation (Fig. S1(c)). Compared with stretchable bulk-like AgNWs electrodes [25, 29], the thin AgNWs network exhibited percolative behaviour which renders the transmittance of electrodes as high as 95% (Fig. S1(d)) with the sheet resistance as low as 54 ohm/sq [19, 30]. The stripe electrodes were obtained by wiping off the AgNWs that were uncovered by the mask, which is an efficient and simple method for large scale fabrication (Fig. S2, in the ESM). Figure 1(c) shows the transmittance of three different parts of as-fabricated devices—which were acquired from the monolayer AgNWs network covered area, the overlapping area and the interspace area—with transmittance of 81%, 77%, and 85%, respectively, at the wavelength of 550 nm. A photograph of the bent film is shown in the inset. From the enhanced contrast picture in Fig. S1(d) (inset), the AgNWs electrode stripes with line width and separation space ~4 mm can be clearly seen, and these parameters can be customized to meet a specified resolution.

The response mechanism of the device is based on a capacitive sensing scheme. However, two types of capacitance, self-capacitance (C_s) and mutual capacitance (C_m) [31, 32], coexist in the device, and Fig. 1(d) shows the schematic image and corresponding equivalent circuit of the capacitive sensor in measurements. Specifically, C_s, the capacitance of the AgNWs electrode stripe with respect to ground, is significantly increased by forming parasitic capacitance (C_p) between the electrode and an approaching object, such as human fingers [33]. Although the proximity sensor in the C_s implementation enables us to detect the location of an approaching object by identifying the row

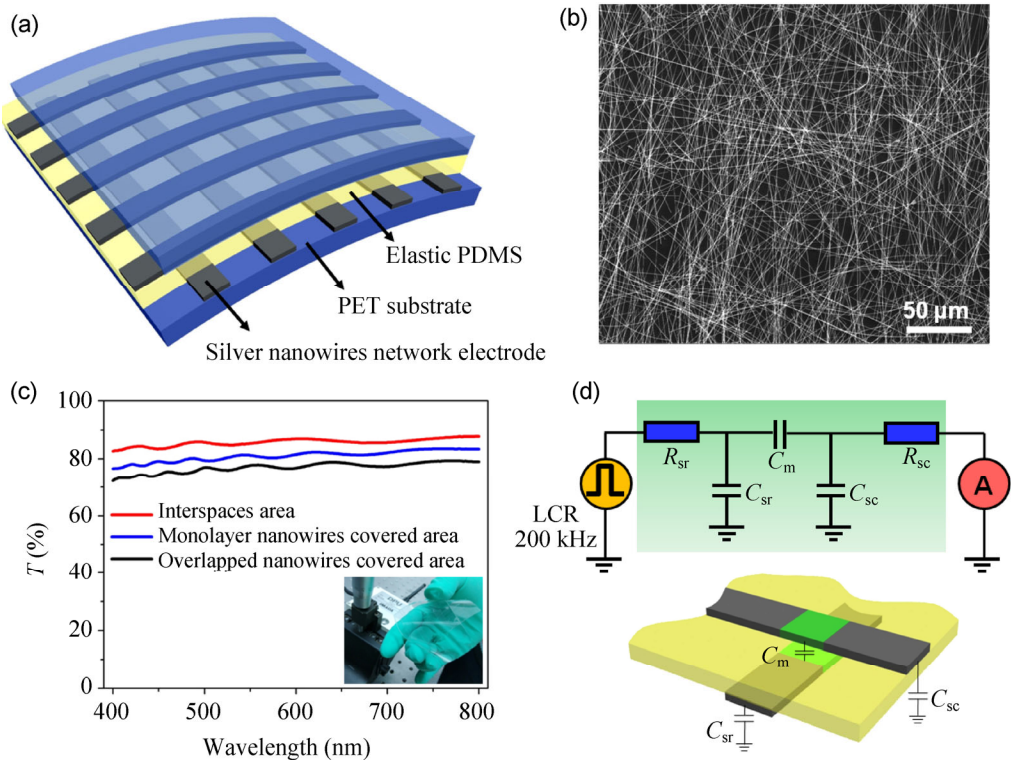

Figure 1 Characterization of the structure and equivalent circuit of the sensor. (a) Schematic illustration of the sandwich structure sensor, with the AgNWs network stripes used as the row and column electrodes arranged orthogonally on the top and bottom PET substrates. (b) The corresponding SEM image of the AgNWs network. (c) Transmittance curves of different areas of the device. (d) Equivalent circuit of the capacitive sensor in measurements (C_{sr} and C_{sc} denote the C_s of row and column electrodes, respectively, and R_{sr} and R_{sc} denote the equivalent resistance of row and column electrodes, respectively).

and column electrodes with the largest changes in capacitance, its high susceptibility to environmental interference—such as humidity, air velocity, and even human body movement (Fig. S3, in the ESM)—hampered qualitative analysis in practical applications. Furthermore, a bigger issue is the appearance of ghost points for multi-point object detection, which result from the virtual intersections in locations other than where the objects are really located [31, 32]. These problems limit the applications of C_s-based proximity sensing. In comparison, C_m can be considered as the capacitance between two charge-holding objects, i.e. the overlapping intersections of AgNWs electrode stripes, which is relatively stable due to the sealed capacitive structure with accessible measurement. Thus the ghost points can be eliminated, allowing accurate multiple-point location identification, as we demonstrate in the following.

As shown in Fig. 2(a), when a grounded conductive object (a finger was used here to simulate the real environment) came close to an intersection (as illustrated in the inset), the change of C_m (ΔC, denoting the absolute capacitance change) depended on the change of height d (the distance from the intersection to the finger tip), and the rate of C_m change is defined as $\Delta C/C_0$, where C_0 denotes the original C_m. The baseline of C_m for the device-under-test without proximity or pressure was 3.054 pF, and this value varied for different devices. In principle, with the proximity of a finger, the shortened d should result in the increase of C_p between the finger and electrode, because the electric field between the two electrodes at the intersection will be disturbed by the finger and some of the electric field will be shunted, thus reducing the measured C_m as illustrated in Fig. 2(b) [34]. That is to say, C_m increased with increasing d while C_s had the opposite trend. As seen in Fig. 2(a), the C_m changed more obviously for small d, implying higher sensitivity in this range. We compared the experimental results and values simulated using effective theory [35] to fit

the change in $\Delta C/C_0$ (Fig. S4, in the ESM), and found that for close proximity detection ($d < 4$ cm), the theoretical values and measured values are more consistent, which is probable due to the prominent influence of C_p on the C_m, while for distant proximity detection, the deviation becomes larger since the interference of the surrounding environment on the objects cannot be neglected. The corresponding response of five adjacent intersections to a single hovering finger is shown in Fig. 2(c) using a contour map, which clearly demonstrates the variation of C_m with d. The central dashed box is the intersection position (pixel) where the finger is hovering right above, and the other dashed boxes correspond to adjacent pixels. When d decreases from 3 to 0.5 cm, the most significant change in $\Delta C/C_0$ can be observed in the center. We note that the $\Delta C/C_0$ of the left and right pixels are larger than the values for the top and bottom ones (bottom panel in Fig. 2(c)), which is because the finger has an oval shape rather than the standard circle, indicating the excellent geometric discrimination capability of the device.

In order to study the response performance of the sensor, Fig. 2(d) shows the capacitance variations when a finger approached and moved away for four cycles; the device showed good reversibility and stability with fast response, which offers the possibility to achieve precise proximity detection. It is worth mentioning that, by virtue of the unique measurement mechanism, proximity sensing based on C_m can avoid the advent of the ghost points and allow theoretically unlimited object detection with unambiguous location identification [36]. To demonstrate the good spatial resolution and multi-point proximity sensing, two hovering metal bars (cross-section diameter ~1 cm^2) were placed right above the adjacent pixels of a 64-pixel sensor (marked by the black dashed box with h ~1 cm) as seen in Fig. 2(e). Notable changes of

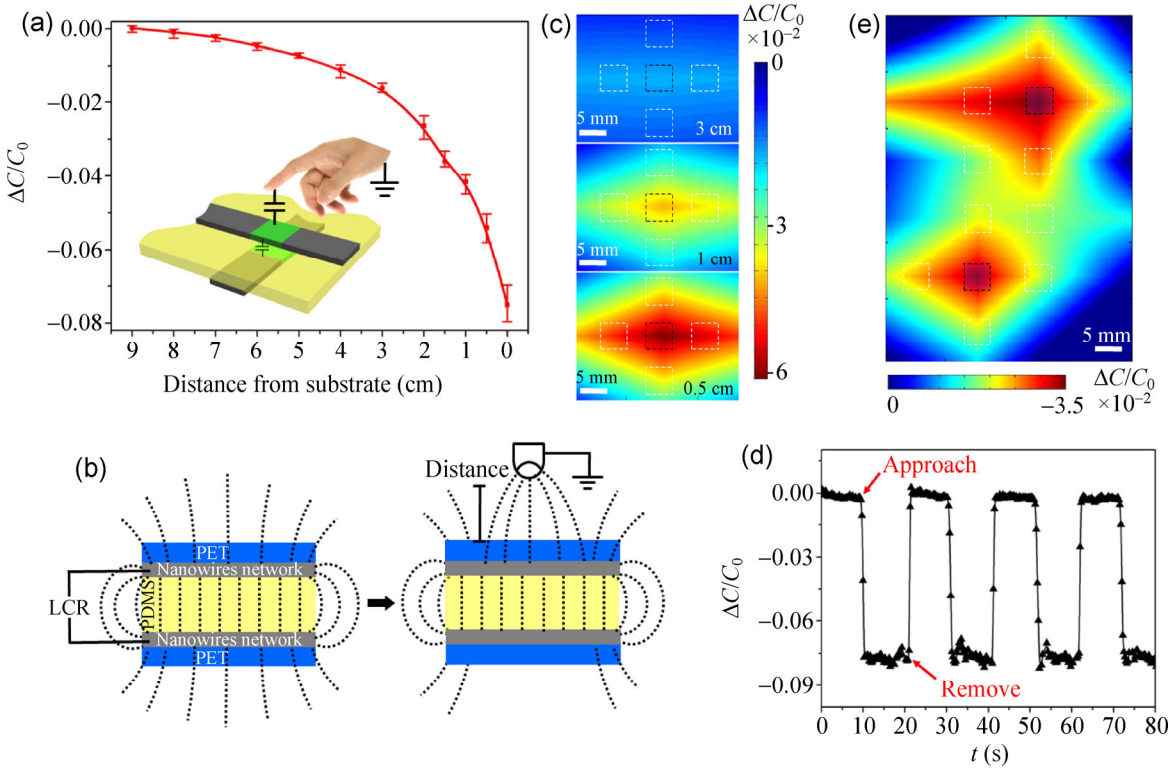

Figure 2 Characterization of the capacitive proximity response of matrix-structured sensor. (a) Change in capacitance ($\Delta C/C_0$) versus height d (vertical distance from the overlapping intersection of AgNWs electrodes to the finger tip). (b) Schematic images of a hovering finger's influence on C_m. (c) Contour images of the estimated capacitance change profile of a central pixel and its four nearest neighbors when a finger approached with different d (3, 1 and 0.5 cm). (d) Plot of $\Delta C/C_0$ versus response time with approaching and moving away for four cycles. (e) Proximity sensing to two metal bars with d ~1 cm, with the intersections marked by black dashed boxes.

$\Delta C/C_0$ in these two areas can be clearly observed from the contour image, and the excellent independent response of each pixel without crosstalk is a benefit of the C_m based sensing mode, which indicates its potential applications in non-touch multi-point gesture operation for a screen. In principle, the space distance between the adjacent pixels decides the spatial resolution of the sensor (the width of the AgNWs electrode stripes and their interval distance). Moreover, improvements in manufacturing technique can narrow the size of the electrode and interval space, which can enhance the spatial resolution, although the base C_m of each pixel would decrease.

Apart from precise proximity detection, the C_m based sensor can handle detection in the contact mode and can serve as a pressure sensor as well [22, 24, 37], which cannot be realized in a C_s based sensor. In brief, each intersection in the matrix-structure represents a unit of a simplified parallel-plate capacitor and its capacitance is proportional to $1/D$, where D is the thickness of the PDMS dielectric layer. When the device was subjected to pressure, the PDMS layer was compressed, thus D decreased, and Fig. 3(a) shows the $\Delta C/C_0$ changed with increasing pressure. In the low-pressure range (up to 50 kPa), $\Delta C/C_0$ was linearly dependent on pressure (Fig. 3(a) inset), while at higher pressures the slope gradually became flat and the pressure tended to be saturated, owing to the increasing elastic resistance of PDMS. Comparing with a previously reported result [4], the pressure sensitivity S (defined as the slope of the curve, $S = \delta(\Delta C/C_0)/\delta P$) of our device is not very high (~0.4 MPa^{-1}); this is due to the relatively compact structure of the flat PDMS layer (Poisson ratio 0.5, Young's modulus 750 kPa). The sensitivity could be improved by fabricating microstructure on the PDMS films [4], but this would

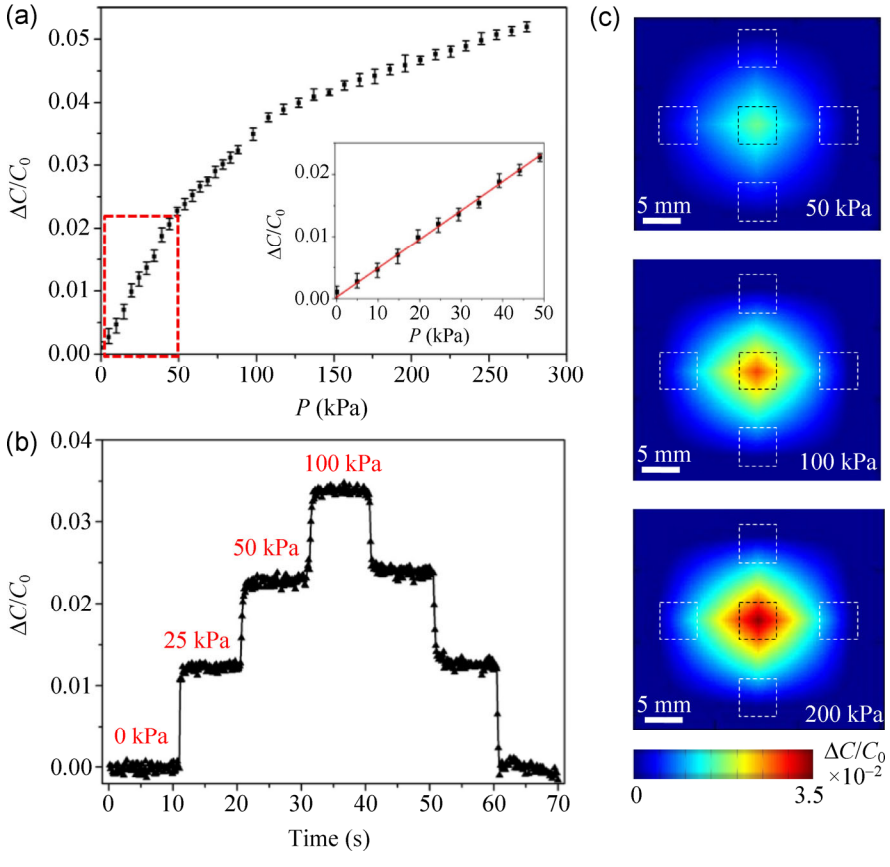

Figure 3 Characterization of the capacitive pressure response of matrix-structured sensor. (a) Plot of $\Delta C/C_0$ versus applied pressure up to 260 kPa (the inset shows the linear relationship up to 50 kPa). (b) The reversible response of $\Delta C/C_0$ to the applied step-up and step-down pressures (0, 25, 50, and 100 kPa). (c) Contour images of the estimated capacitance change profile of a central pixel and its four nearest neighbors when the central pixel was loaded with different pressures (50, 100 and 200 kPa).

decrease the high transmittance of the film because of the resulting light scattering, and its desirability would depend on the specific application. In addition, the sensor could retain high stability and reversibility even when subjected to high pressure up to 100 kPa, and the fast capacitance switching with applied step-up and step-down pressures showed symmetric jumps without hysteresis (Fig. 3(b)), while the durability test demonstrated its steady response to a 100 kPa, 2 Hz pressure for 200 cycles (Fig. S5, in the ESM). This large dynamic range of detectable pressure and stable performance make the device capable of withstanding harsh industrial field environments. We also studied the spatial resolution in the pressure sensing, as shown in Fig. 3(c) [38, 39]. When applying a pressure (1 cm^2 square of glass sheet), the $\Delta C/C_0$ of the central pixel where the load applied is around six times higher than the average for adjacent pixels, and thus the pressure location can be determined easily. The tiny increase of $\Delta C/C_0$ for the adjacent four pixels is probably due to the pressure causing a geometric shape deformation.

To study the response switching between two sensing modes, we precisely measured the C_m change during the overall process from proximity sensing to pressure sensing, and then returning to the original state for two cycles using a 3D movable platform as seen in Fig. 4; the corresponding steps are schematically shown in the insets. The device performed well during the whole process with seamless switching. The turning points marked by the circles denote the positions where the object just touched the sensor, and serve as the switching point. In our measurement, the proximity induced C_m change does not result in a crosstalk with that generated by pressure, because although the C_m changes induced in these two ways are of the same order of magnitude, they have opposite dependence on the direction of movement of the object. Moreover, d was constant during the pressure loading, and thus the proximity induced C_m change is negligible. In practical applications, when a finger touches the sensor, this will inevitably result in pressure after touching, and if the control system detects the turning point, it can judge the switch from proximity mode to pressure mode successfully; a similar situation applies for the reverse process. Therefore, non-contact detection (proximity sensing) or contact detection (pressure sensing) can be easily and clearly identified through determining the turning point, and the pressure value and proximity height can be obtained as well. In addition, considering the high sensitivity of capacitive response in the vicinity of the turning point, switching occurs readily, and thus erroneous judgments can be effectively avoided.

3 Conclusion

Our technical goal is to implement a monolithically integrated dual functional sensor with high transparency, which can detect the objects in both non-contact and

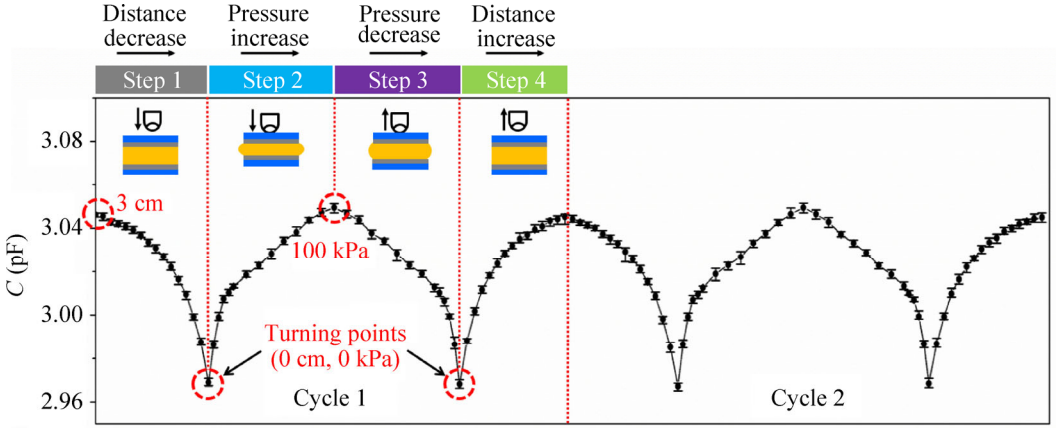

Figure 4 The overall response between proximity and pressure sensing with seamless switching. Each cycle contains four steps, (step 1) approaching from 3 to 0 cm, (step 2) applying pressure up to 100 kPa, (step 3) releasing and (step 4) returning back to the original position.

mechanical contact modes. The C_m-based sensor we have demonstrated here is a qualified candidate for this purpose. It can sense proximity and pressure in one device and make a seamless switch and precise response to the overall physical process with a fast response, high stability and high reversibility. Meanwhile, the good isolation of each pixel in the matrix-structure leads to accurate spatial sensing and location identification. With refinement [40], this powerful integrated proximity–contact sensor can be applied in smart phones, game machines and robots, but is not limited to these.

4 Experimental

4.1 Synthesis of AgNWs ink

The AgNWs was synthesized followed previous work [19]. Polyvinyl pyrrolidone (PVP) (0.26 g, M_W = ~1,300,000) and $FeCl_3$ (0.15 mg) were added sequentially to a vessel and mixed with ethylene glycol (50 mL), and then the mixture was stirred moderately for 10 min. The solution was then heated at 180 ℃ for half an hour in an oven, and then cooled down to room temperature in a glass dryer. $AgNO_3$ powder (0.1168 g) was then added to the solution with vigorous stirring for 10 min until it was fully dissolved. Then the solution was sealed in a bottle and kept at 145 ℃ for 7 h in the oven. Finally, the obtained products were washed with acetone and alcohol several times, and stored in alcohol before use. The morphology, structure, and composition of the samples were probed by a scanning electron microscope (SEM, FEI Nova NanoSEM 450).

4.2 Electrical and optical measurements

We measured C_m with a LCR meter (HIOKI IM3533-1) with 200 kHz AC signal source, and the variation of C_m with pressure was measured by applying a compressive force perpendicular to the film which was placed between a force gauge and a movable platform with a glass slide placed on it (contact area ~1 cm^2). The curve of C_m versus d was plotted through adjusting d of the conductive objects, which were fastened onto the movable platform with a ruler with millimetre precision (including finger and metal bar, only conductive objects were considered in the sensor analyses). The optical transmission of the AgNWs network film was measured using a UV2550 spectrophotometer, and all the values of transmission were in the visible light spectrum (400–800 nm), and the transmission of AgNWs network deposited PET sheet was taken at 550 nm.

4.3 Generation of the capacitance change contour map

The contour maps of single-point proximity sensing and pressure sensing were generated according to the data of the central pixel where proximity or pressure was applied, and the data from the adjacent four pixels. The map of double-point proximity was created based on two central pixels with all the adjacent pixels and intermediate pixels. A simple bilinear interpolation was applied to estimate capacitance change in order to create a data table and convert into a contour map.

Acknowledgements

This work was supported by the National Natural Science Foundation of China (No. 61204001), and the Fundamental Research Funds for the Central Universities of China (No. 2014QN013). We also thank the Center for Nanoscale Characterization & Devices (CNCD), WNLO of HUST for the use of facilities in support of this work.

Electronic Supplementary Material: Supplementary material (details of AgNWs deposition and performance, fabrication of the matrix-structure capacitive sensor, the response of C_m and C_s to the environmental interference, the use of effective theory to deal with the parasitic capacitance analysis, and cycle durability tests) is available in the online version of this article at http://dx.doi.org/10.1007/s12274-014-0510-3.

References

[1] Maheshwari, V.; Saraf, R. F. High-resolution thin-film device to sense texture by touch. *Science* **2006**, *312*, 1501–1504.

[2] Hu, B.; Chen, W.; Zhou, J. High performance flexible sensor based on inorganic nanomaterials. *Sensor. Actuat. B* **2013**, *176*, 522–533.

[3] Hu, B.; Ding, Y.; Chen, W.; Kulkarni, D.; Shen, Y.; Tsukruk, V. V.; Wang, Z. L. External-strain induced insulating phase transition in VO_2 nanobeam and its application as flexible strain sensor. *Adv. Mater.* **2010**, *22*, 5134–5139.

[4] Mannsfeld, S. C.; Tee, B. C. K.; Stoltenberg, R. M.; Chen, C. V. H. H.; Barman, S.; Muir, B. V. O.; Sokolov, A. N.; Reese, C.; Bao, Z. N. Highly sensitive flexible pressure sensors with microstructured rubber dielectric layers. *Nat. Mater.* **2010**, *9*, 859–864.

[5] Wu, W. Z.; Wen, X. N.; Wang, Z. L. Taxel-addressable matrix of vertical-nanowire piezotronic transistors for active and adaptive tactile imaging. *Science* **2013**, *340*, 952–957.

[6] Tee, B. C. K.; Wang, C.; Allen, R.; Bao, Z. N. An electrically and mechanically self-healing composite with pressure- and flexion-sensitive properties for electronic skin applications. *Nat. Nanotechnol.* **2012**, *7*, 825–832.

[7] Wang, C.; Hwang, D.; Yu, Z. B.; Takei, K.; Park, J.; Chen, T.; Ma, B. W.; Javey, A. User-interactive electronic skin for instantaneous pressure visualization. *Nat. Mater.* **2013**, *12*, 899–904.

[8] Ramuz, M.; Tee, B. C. K.; Tok, J. B. H.; Bao, Z. N. Transparent, optical, pressure-sensitive artificial skin for large-area stretchable electronics. *Adv. Mater.* **2012**, *24*, 3223–3227.

[9] Lee, H. K.; Chang, S. I.; Yoon, E. Dual-mode capacitive proximity sensor for robot application: Implementation of tactile and proximity sensing capability on a single polymer platform using shared electrodes. *IEEE Sens. J.* **2009**, *9*, 1748–1755.

[10] Sadler, D. J.; Ahn, C. H. On-chip eddy current sensor for proximity sensing and crack detection. *Sensor. Actuat. A* **2001**, *91*, 340–345.

[11] Gueissaz, F.; Piguet, D. The microreed, an ultra-small passive MEMS magnetic proximity sensor designed for portable applications. In *The 14th IEEE International Conference on Micro Electro Mechanical Systems*, Interlaken, Switzerland, 2001, pp 269–273.

[12] Canali, C.; De Cicco, G.; Morten, B.; Prudenziati, M.; Taroni, A. A temperature compensated ultrasonic sensor operating in air for distance and proximity measurements. *IEEE Trans. Ind. Electron.* **1982**, *IE-29*, 336–341.

[13] Balek, D.; Kelley, R. Using gripper mounted infrared proximity sensors for robot feedback control. In *1985 IEEE International Conference on Robotics and Automation*, St. Louis, USA, 1985, pp 282–287.

[14] Chen, Z. H.; Luo, R. C. Design and implementation of capacitive proximity sensor using microelectromechanical systems technology. *IEEE Trans. Ind. Electron.* **1998**, *45*, 886–894.

[15] Takamatsu, S.; Yamashita, T.; Imai, T.; Itoh, T. Fabric touch sensors using projected self-capacitive touch technique. *Sens. Mater.* **2013**, *25*, 627–634.

[16] Kim, H. K.; Lee, S.; Yun, K. S. Capacitive tactile sensor array for touch screen application. *Sensor. Actuat. A* **2011**, *165*, 2–7.

[17] Guo, S. W.; Guo, J.; Ko, W. H. A monolithically integrated surface micromachined touch mode capacitive pressure sensor. *Sensor. Actuat. A* **2000**, *80*, 224–232.

[18] Ko, W. H.; Wang, Q. Touch mode capacitive pressure sensors. *Sensor. Actuat. A* **1999**, *75*, 242–251.

[19] Zhu, S. W.; Gao, Y.; Hu, B.; Li, J.; Su, J.; Fan, Z. Y.; Zhou, J. Transferable self-welding silver nanowire network as high performance transparent flexible electrode. *Nanotechnology* **2013**, *24*, 335202.

[20] Lee, J.; Lee, P.; Lee, H.; Lee, D.; Lee, S. S.; Ko, S. H. Very long Ag nanowire synthesis and its application in a highly transparent, conductive and flexible metal electrode touch panel. *Nanoscale* **2012**, *4*, 6408–6414.

[21] De, S.; Higgins, T. M.; Lyons, P. E.; Doherty, E. M.; Nirmalraj, P. N.; Blau, W. J.; Boland, J. J.; Coleman, J. N. Silver nanowire networks as flexible, transparent, conducting films: Extremely high DC to optical conductivity ratios. *ACS Nano* **2009**, *3*, 1767–1774.

[22] Lipomi, D. J.; Vosgueritchian, M.; Tee, B. C. K.; Hellstrom, S. L.; Lee, J. A.; Fox, C. H.; Bao, Z. N. Skin-like pressure and strain sensors based on transparent elastic films of carbon nanotubes. *Nat. Nanotechnol.* **2011**, *6*, 788–792.

[23] Vandeparre, H.; Watson, D.; Lacour, S. P. Extremely robust and conformable capacitive pressure sensors based on flexible polyurethane foams and stretchable metallization. *Appl. Phys. Lett.* **2013**, *103*, 204103.

[24] Hu, W. L.; Niu, X. F.; Zhao, R.; Pei, Q. B. Elastomeric transparent capacitive sensors based on an interpenetrating composite of silver nanowires and polyurethane. *Appl. Phys. Lett.* **2013**, *102*, 083303.

[25] Yao, S. S.; Zhu, Y. Wearable multifunctional sensors using printed stretchable conductors made of silver nanowires. *Nanoscale* **2014**, *6*, 2345–2352.

[26] Hecht, D. S.; Hu, L. B.; Irvin, G. Emerging transparent electrodes based on thin films of carbon nanotubes, graphene, and metallic nanostructures. *Adv. Mater.* **2011**, *23*, 1482–1513.

[27] Hu, L. B.; Kim, H. S.; Lee, J. Y.; Peumans, P.; Cui, Y. Scalable coating and properties of transparent, flexible, silver nanowire electrodes. *ACS Nano* **2010**, *4*, 2955–2963.

[28] Kim, T. Y.; Kim, Y. W.; Lee, H. S.; Kim, H.; Yang, W. S.; Suh, K. S. Uniformly interconnected silver-nanowire networks for transparent film heaters. *Adv. Funct. Mater.* **2013**, *23*, 1250–1255.

[29] Xu, F.; Zhu, Y. Highly conductive and stretchable silver nanowire conductors. *Adv. Mater.* **2012**, *24*, 5117–5122.

[30] Bergin, S. M.; Chen, Y. H.; Rathmell, A. R.; Charbonneau, P.; Li, Z. Y.; Wiley, B. J. The effect of nanowire length and diameter on the properties of transparent, conducting nanowire films. *Nanoscale* **2012**, *4*, 1996–2004.

[31] Barrett, G.; Omote, R. Projected-capacitive touch technology. *Information Display* **2010**, *3*, 16–21.

[32] Wang, T.; Blankenship, T. Projected capacitive touch systems from the controller point of view. *Information Display* **2011**, *3*, 8–11.

[33] Tartagni, M.; Guerrieri, R. A fingerprint sensor based on the feedback capacitive sensing scheme. *IEEE J. Solid-State Circuits* **1998**, *33*, 133–142.

[34] Cotton, D. P. J.; Graz, I. M.; Lacour, S. P. A multifunctional capacitive sensor for stretchable electronic skins. *IEEE Sens. J.* **2009**, *9*, 2008–2009.

[35] Li, N.; Zhu, H. Y.; Wang, W. Y.; Gong, Y. Parallel double-plate capacitive proximity sensor modelling based on effective theory. *AIP Adv.* **2014**, *4*, 027119.

[36] Ko, S.; Shin, H.; Lee, J.; Jang, H.; So, B. C.; Yun, I.; Lee, K. Low noise capacitive sensor for multi-touch mobile handset's applications. In *2010 IEEE Asian Solid-State Circuits Conference (A-SSCC)*, Beijing, China, 2010, pp 1–4.

[37] Yamada, T.; Hayamizu, Y.; Yamamoto, Y.; Yomogida, Y.; Izadi-Najafabadi, A.; Futaba, D. N.; Hata, K. A stretchable carbon nanotube strain sensor for human-motion detection. *Nat. Nanotechnol.* **2011**, *6*, 296–301.

[38] Someya, T.; Sekitani, T.; Iba, S.; Kato, Y.; Kawaguchi, H.; Sakurai, T. A large-area, flexible pressure sensor matrix with organic field-effect transistors for artificial skin applications. *Proc. Natl. Acad. Sci. USA* **2004**, *101*, 9966–9970.

[39] Kane, B. J.; Cutkosky, M. R.; Kovacs, G. T. A traction stress sensor array for use in high-resolution robotic tactile imaging. *J. Microelectromech. Syst.* **2000**, *9*, 425–434.

[40] He, M. X.; Liu, R.; Li, Y.; Wang, H.; Lu, X.; Ding, G. F.; Wu, J. J.; Zhang, T.; Zhao, X. L. Tactile probing system based on micro-fabricated capacitive sensor. *Sensor. Actuat. A* **2013**, *194*, 128–134.